

Communication

Kaon Femtoscopy with Lévy-Stable Sources from $\sqrt{s_{NN}} = 200$ GeV Au + Au Collisions at RHIC

Ayon Mukherjee 

Department of Atomic Physics, Eötvös Loránd University (ELTE), Pázmány Péter Stny. 1/A,
H-1117 Budapest, Hungary; ayon.mukherjee@ttk.elte.hu

Abstract: Femtoscopy has the capacity to probe the space-time geometry of the particle-emitting source in heavy-ion collisions. In particular, femtoscopy of like-sign kaon pairs may shed light on the origin of non-Gaussianity of the spatial emission probability density. The momentum correlations between like-sign kaon pairs are measured in data recorded by the STAR experiment, from $\sqrt{s_{NN}} = 200$ GeV Au + Au collisions at RHIC, BNL. Preliminary results hint at the possible existence of non-Gaussian, Lévy-stable sources, with the likely presence of an anomalous diffusion process in the signal for the identically charged kaon pairs so produced. More statistically significant studies at lower centre-of-mass energies may contribute to the search for the critical end point of QCD.

Keywords: RHIC; STAR; femtoscopy; Bose–Einstein correlations; Lévy distribution; anomalous diffusion; identically charged kaons; heavy-ion collisions; high-energy physics

1. Introduction

Following the discovery of quark–gluon plasma, one of the main thrusts of high-energy nuclear physics has been the understanding and exploration of the space-time geometry of the particle-emitting source created in heavy-ion collisions [1]. The quantity mainly investigated to this end is the two-particle source function, sometimes called the spatial correlation function (CF) or the pair-source distribution. Although this quantity is not easy to reconstruct experimentally, detailed studies of its behaviour are merited by a multitude of reasons, including its connections to hydrodynamic expansion [2,3], critical phenomena [4], light nuclei formation [5], etc. Phenomenological studies and experimental analyses both, emphasise the importance of describing the shape of the source function. Previously conducted hydrodynamical studies seem to suggest a Gaussian source shape [3,6]. Multiple measurements were also taken with the Gaussian assumption [7,8]. However, recent source-imaging studies suggest that the two-particle source function for pions has a long-range component, obeying power-law behaviour [9–14].

Femtoscopy [15] is the sub-field of high-energy heavy-ions physics that allows for the investigation of the space-time structure of femtometre-scale processes encountered in high-energy nuclear and particle physics experiments. Femtoscopic correlations in heavy-ion collisions are currently understood to be caused partly by Bose–Einstein statistics [16–19]. Alternatively, they are called Hanbury-Brown–Twiss (HBT) correlations in recognition of pioneering works by Hanbury-Brown and Twiss [21, 22] on intensity interferometry in the field of observational astronomy to extract the apparent angular sizes of stars from correlations between the signals of two detectors. Additionally, correlations can arise out of final-state interactions, such as electromagnetic interactions and strong interactions undergone by the investigated particles. These correlations between pairs of identical bosons can be used to explore the properties of the matter created in heavy-ion collisions and to map the geometry of the particle-emitting source [1].



Citation: Mukherjee, A. Kaon Femtoscopy with Lévy-Stable Sources from $\sqrt{s_{NN}} = 200$ GeV Au + Au Collisions at RHIC. *Universe* **2023**, *9*, 300. <https://doi.org/10.3390/universe9070300>

Academic Editor: Jun Xu

Received: 27 May 2023

Revised: 17 June 2023

Accepted: 20 June 2023

Published: 22 June 2023



Copyright: © 2023 by the authors. Licensee MDPI, Basel, Switzerland. This article is an open access article distributed under the terms and conditions of the Creative Commons Attribution (CC BY) license (<https://creativecommons.org/licenses/by/4.0/>).

2. Correlations

Femtoscopy works on the principle that the momentum correlation function of a pair of particles is related to the probability density of particle creation at a space-time point (X) for a particle with four-momentum P . This probability density ($S(X, P)$) is also called the source function. Defining $N_1(P)$ —obtained by multiplying the particle-creation probability density by $\langle n \rangle$, the average number of particles—as the momentum-invariant distribution and $N_2(P_1, P_2)$ —obtained by multiplying the pair-creation probability density by $\langle n(n - 1) \rangle$, the average number of pairs—as the pair-momentum distribution, the two-particle correlation function can be written as [23]:

$$C(P_1, P_2) = \frac{N_2(P_1, P_2)}{N_1(P_1)N_1(P_2)} ; \tag{1}$$

where

$$N_2(P_1, P_2) = \int S(X_1, P_1)S(X_2, P_2) |\psi_{P_1, P_2}(X_1, X_2)|^2 d^4X_1 d^4X_2 , \tag{2}$$

where $\psi_{P_1, P_2}(X_1, X_2)$ is the two-particle wave function that simplifies to:

$$|\psi_{P_1, P_2}(X_1, X_2)|^2 = \left| \psi_{P_1, P_2}^{(0)}(X_1, X_2) \right|^2 = 1 + \cos[(P_1 - P_2)(X_1 - X_2)] \tag{3}$$

in the interaction-free case for bosons, when only the quantum-statistical effects are taken into account. Thus, the correlation function can be redefined as [24]:

$$C(Q, K) \simeq 1 + \frac{|\tilde{S}(Q, K)|^2}{|\tilde{S}(0, K)|^2} ; \tag{4}$$

where

$$Q = P_1 - P_2 , K = \frac{P_1 + P_2}{2} \tag{5}$$

and

$$\tilde{S}(Q, K) = \int S(X, K) e^{iQX} d^4X \tag{6}$$

denote the pair-momentum difference, the average momentum and the Fourier transform (FT) of the source, respectively, assuming that $Q \ll K$ holds for the kinematic range under investigation. The correlation functions are measured with respect to Q over a range of well-defined K values; then, the properties of the correlation functions are analysed as functions of the average K for each of those ranges.

A significant fraction of the particles created in a heavy-ion collision is secondary, i.e., they come from decay. Whereas the primordial particles are created directly from the hydrodynamic expansion of the collision volume, the decay particles arise from interactions that take place much later. Hence, the source can be assumed to consist of the following two components [25]:

1. a core ($S_C(X, K)$) consisting of primordial particles created by the hydrodynamically expanding, strongly interacting quark–gluon plasma, along with the decays of resonances with half lives of less than a few fm/c; and
2. a halo ($S_H(X, K)$) consisting of the products created by the decay of long-lived resonances, including but not limited to η, η', K_S^0 and ω , making it possible to decompose $S(X, K)$ as [25]:

$$S(X, K) = S_C(X, K) + S_H(X, K). \tag{7}$$

As explained in detail in Ref. [25], the Fourier-transformed emission function of the halo vanishes for resolvable relative momenta, i.e., the Q values that lie in the experimentally achievable region. Hence, the halo does not contribute to the measured correlation function, which, in turn, is determined by the core component. Hence, the measured correlation function, when extrapolated to $Q = 0$, does not take a value of 2 as expected from Equation (4) but takes the following form:

$$\lim_{Q \rightarrow 0} C(Q, K) = 1 + \lambda(K) < 2. \tag{8}$$

This “intercept parameter” of the correlation function, also called the correlation strength ($\lambda(K)$) may depend on the pair-momentum K . It can be understood on the basis of the core-halo model by rewriting the correlation function using Equations (4), (6) and (7); and the fact that $\tilde{S}_H(Q, K) \approx 0$ for experimentally accessible values of Q [9]:

$$\begin{aligned} C(Q, K) &= 1 + \left[\frac{N_C(K)}{N_C(K) + N_H(K)} \right]^2 \frac{|\tilde{S}_C(Q, K)|^2}{|\tilde{S}_C(0, K)|^2} \\ &= 1 + \lambda(K) \frac{|\tilde{S}_C(Q, K)|^2}{|\tilde{S}_C(0, K)|^2}, \end{aligned} \tag{9}$$

where $N_C(K) = \int S_C(X, K) d^4X$ and $N_H(K) = \int S_H(X, K) d^4X$ are contributions of the core and the halo, respectively, and $\lambda(K)$ is:

$$\lambda(K) = \left[\frac{N_C(K)}{N_C(K) + N_H(K)} \right]^2. \tag{10}$$

Realising that $X \equiv X(\vec{r}, t)$, the spatial correlation function:

$$D(\vec{r}, K) = \int S(\vec{r}' + \frac{\vec{r}}{2}, K) S(\vec{r}' - \frac{\vec{r}}{2}, K) d^3\vec{r}' \tag{11}$$

can be used to rewrite $C(Q, K)$ as [24]:

$$C(Q, K) \approx \frac{\int D(\vec{r}, K) |\psi_Q(\vec{r})|^2 d^3\vec{r}}{\int D(\vec{r}, K) d^3\vec{r}}. \tag{12}$$

3. Lévy Distribution

Usually, the shape of the source distribution is assumed to be Gaussian. However, evidence of a non-Gaussian source for correlated pions has been found in multiple studies, necessitating a generalisation of the distribution to a Lévy-stable one [26]:

$$S(x, K) = \mathcal{L}(x; \alpha, \lambda, R) = \frac{1}{2\pi} \int e^{-(Q'R)^\alpha} e^{iQ'x} dQ'; \tag{13}$$

where \mathcal{L} is the one-dimensional Lévy function, R is the Lévy-scale parameter, λ is the correlation strength, $0 < \alpha \leq 2$ is the Lévy exponent and Q' is the integration variable. These parameters are generally understood to depend on K . Salient features of the distribution include moments greater than α being undefined and $D(\vec{r}, K)$ necessarily having a Lévy shape with the same α in cases in which $S(X, K)$ is Lévy-shaped. The distribution exhibits a power-law behaviour for $\alpha < 2$, where $\alpha = 1$ represents a Cauchy distribution and $\alpha = 2$ represents a Gaussian distribution. Multiple factors, such as anomalous diffusion, jet fragmentation and proximity to the critical end point (CEP), can contribute to the appearance of Lévy-stable sources. However, the high-multiplicity, nucleon-on-nucleon nature of the analysed heavy-ion collisions makes it unlikely for jet fragmentation to be the dominant reason for the appearance of Lévy sources in this study—as it has been identified as the cause of Lévy-stable sources in e^+e^- collisions at LEP [13]. On the other hand, the high centre-of-mass-energy of the collisions explored here rules out the possibility of the system being close to the critical end point [4,27,28].

Interestingly, it is trivial to establish that α is related to one of the critical exponents (η). In the case of a second-order phase transition, the η exponent describes the power-law behaviour of the spatial correlation function at the critical end point with an exponent of $-(d - 2 + \eta)$, where d is the dimension. In a three-dimensional analysis in which $d = 3$, this exponent would compute to $-(1 + \eta)$. However, it is established that the three-dimensional

Lévy distribution describes the power-law tail of the spatial correlation function with an exponent of $-(1 + \alpha)$. Thus, comparing the exponents at the critical end point, it can be easily seen that the Lévy exponent (α) is identical to the critical exponent (η), a conjecture explored in Ref. [29]. The second-order QCD phase transition is expected to be in the same universality class as the three-dimensional Ising model. In that case, the η exponent has a value of 0.03631 ± 0.00003 at the critical end point [30]. However, the universality class of the random-field, three-dimensional Ising model may also be of relevance here, where the value of η is 0.50 ± 0.05 [31]. Thus, extracting α at collision energies lower than those used in this analysis while taking into account finite size and time effects might yield insightful information about the nature of the quark–hadron phase transition and shed light on the location of the critical end point in the QCD phase diagram [4,32–35].

As coordinate-space distributions extracted from experimental data show a heavy tail, the limitations of the hydrodynamical approach—assuming idealised freeze-out with a sudden jump in the mean free path from zero to infinity—become clear. This requires a more realistic approach using hadronic rescattering whereby the system cools as it dilutes with an expanding hadron gas, its mean free path diverges to infinity in a finite time interval and rescattering occurs in the presence of a time-dependent mean free path. This signals the existence of anomalous diffusion—experimentally observed as power-law-shaped tails in coordinate-space distributions of the source—in the system, as opposed to normal diffusion, with the Gaussian source exhibiting a strongly decaying tail caused by the Brownian motion of the particles constituting the system.

The momentum-space diffusion equation of one-dimensional, normal diffusion is expressed as [28]:

$$\frac{\partial W(q, t)}{\partial t} = -k_N q^2 W(q, t); \tag{14}$$

where k_N is the normal-diffusion constant, q is the momentum, t is the time and $W(q, t)$ is the momentum-space probability distribution. The coordinate-space solution to Equation (14) is given by the following Gaussian expression:

$$W(x, t) = \frac{1}{\sqrt{4\pi k_N t}} \exp\left(-\frac{x^2}{4k_N t}\right). \tag{15}$$

For anomalous diffusion, the coordinate-space diffusion equation, in terms of the spatial probability distribution ($W(x, v, t)$), is the generalised Fokker–Planck equation [28]:

$$\frac{\partial W}{\partial t} + v \frac{\partial W}{\partial x} + \frac{F(x)}{m} \frac{\partial W}{\partial v} = \eta_{\alpha'} {}_0D_t^{1-\alpha'} L_{FP} W. \tag{16}$$

where $\eta_{\alpha'}$ is the generalised friction constant of dimension $[\eta_{\alpha'}] = s^{\alpha'-2}$, ${}_0D_t^{1-\alpha'}$ is the Riemann–Liouville operator:

$${}_0D_t^{1-\alpha'} t^p = \left(\frac{\partial}{\partial t}\right) {}_0D_t^{-\alpha'} t^p = \frac{\Gamma(1+p)}{\Gamma(p+\alpha')} t^{p+\alpha'-1} \tag{17}$$

and L_{FP} is the Fokker–Planck operator:

$$L_{FP} = \frac{\partial}{\partial x} \frac{V'(x)}{m\eta_{\alpha'}} + k_A \frac{\partial^2}{\partial x^2}, \tag{18}$$

where $V'(x)$ is related to the force ($F(x)$) by $F(x) = -\frac{dV(x)}{dx}$, as explained in Refs. [36,37].

The momentum-space solution to Equation (16) is given by:

$$W(q, t) = \exp(-tk_A^\alpha |q|^\alpha). \tag{19}$$

where $W(q, t)$ happens to be the FT or the characteristic function of Lévy-stable source distributions, where α is the Lévy exponent from Equation (13) and k_A is the anomalous

diffusion constant. If a centred, spherically symmetric, Lévy-stable source-distribution is assumed and all final-state interactions are neglected, the one-dimensional, two-particle correlation function takes the following simplified form:

$$C(q) = 1 + \lambda \cdot e^{-(qR)^\alpha}, \tag{20}$$

where λ is the correlation strength from Equations (10) and (8), R is the Lévy scale, α is the Lévy exponent and q is the absolute value of the three-momentum difference in the longitudinally co moving system (LCMS) [9]:

$$q = q_{\text{LCMS}} = |\vec{p}_1 - \vec{p}_2|_{\text{LCMS}}. \tag{21}$$

R can be interpreted as the homogeneity length of the particle species, while α represents the extent of the anomalous diffusion occurring in the system. The spherical symmetry in q_{LCMS} is ideal for a one-dimensional analysis of a three-dimensional, spherically symmetric system. Subsequent measurements with higher precision might necessitate a move towards a full, three-dimensional analysis. Until then, the approximations used in Ref. [38] may be utilised for a preliminary analysis.

Momentum correlations of like-sign kaon pairs at $\sqrt{s_{\text{NN}}} = 200$ GeV can be utilised to calculate $C(q)$ and to, consequently, ascertain the shape of the pair-source distribution. If anomalous diffusion is the sole source of non-Gaussianity, then it is expected that the extent of the anomaly will depend on the total cross section or, equivalently, on the mean free path. Since the mean free path is larger for kaons than for pions, the diffusion of the former is expected to be more anomalous in the hadron gas. Hence, the α for kaons (α_κ) is expected to be smaller [28]. Thus, measuring α_κ may shed light on the role of anomalous diffusion in the hadron gas as the origin of the appearance of Lévy distributions.

4. Measurement

The data used for this analysis were obtained from RHIC’s gold-on-gold collisions at a 200 GeV centre-of-mass energy per nucleon pair. The collisions were performed in 2016 and measured by the solenoidal tracker at RHIC (STAR) experiment. The STAR experiment detects multiple particle species emanating from the medium created by the collisions. These different particle species, depending on their mass and charge, produce different shapes when their ionisation energy loss (dE/dx) is plotted as a function of momentum. These shapes can help distinguish the particle species from each other and help isolate the kaons, as observed in Figure 1. For this investigation, the analysis processes about 410 million events in the 0–30% centrality range. They are subjected to strict track and pair selection criteria that, following Ref. [39], include the identification of kaons via energy loss measured by the time-projection chamber (TPC); pair selection based on the fraction-of-merged-hits (FMH) and the splitting-level (SL); and limitations on the track’s momentum, rapidity and distance-of-closest-approach (DCA).

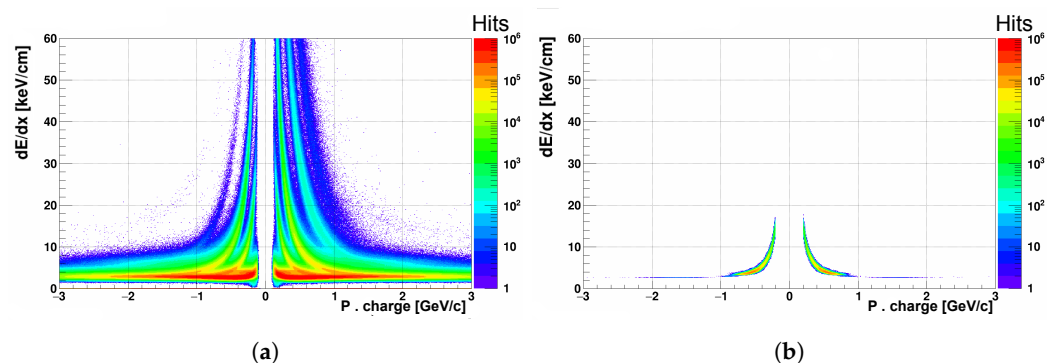


Figure 1. Sample ionisation energy loss as a function of momentum × charge (a) for all available charged particles and (b) after being cut only for the charged kaons to be isolated.

The one-dimensional, like-sign, two-kaon, femtoscopic correlation functions are then experimentally constructed using the event-mixing technique [40]. $A(q)$ —the actual pair distribution—is formed from kaon pairs, with members of the pair belonging to the same event. This distribution is affected by various effects, such as kinematics and acceptance. $B(q)$ —a background distribution—is constructed with the pairs to correct for these effects and the members of this distribution originate from separate events. In this analysis, the method for event mixing described in Refs. [9,13] is used to correct for residual correlations. For a set of event classes based on the centrality and the location of the collision vertex, a background event pool is established. Then, for each real event, a mixed event of the same event class is created from this pool, making sure that each particle in this mixed event belongs to a different real event. Subsequently, pairs within the mixed event contribute to the formation of the aforementioned $B(q)$. Finally, the pre-normalised correlation function is calculated as:

$$C(q) = \frac{A(q)}{B(q)} \cdot \frac{\int B(q) dq}{\int A(q) dq}, \tag{22}$$

for three different ranges of transverse mass (m_T), defined as $m_T = \sqrt{m^2 + (K_T/c)^2}$, where m is the kaon mass and K_T is the average transverse momentum of the pair. The normalisation integrals are performed over a range in which the correlation function is not supposed to exhibit quantum-statistical features. It is to be noted that the method outlined here is applied to pairs belonging to a given range of average momenta. Furthermore, in the event-mixing technique described above, the number of actual and background pairs is the same, aside from the effect of the pair-selection criteria mentioned earlier.

With the momentum correlations, obtained from experimental data (both measured and the empirical values of the calculated correlation function), preparations are made to fit the Lévy function detailed in Equation (20) to $C(q)$. However, the assumptions behind Equation (20) make it unsuitable for a direct fit to experimentally obtained data. As mentioned in Section 1, final-state interactions have considerable effects on the momentum correlations between like-sign kaon pairs; therefore, they need to be imbibed into the analysis as corrections to Equation (20) in order to make it suitable and physically relevant as a fit for the correlation function obtained above. Multiple factors can contribute to the final-state modifications of the momentum correlations, the leading of which are Coulomb interactions, as a gas of charged hadrons can never be entirely devoid of Coulomb repulsion.

The final-state Coulomb interactions are incorporated into the CF by using the Bowler-Sinyukov formula, which includes a correction term for Coulomb repulsion, which is expressed as [41,42]:

$$C(q) = \left[1 - \lambda + \lambda \cdot \mathcal{K}(q; \alpha, R) \cdot \left(1 + e^{-(qR)^\alpha} \right) \right] \cdot N \cdot (1 + q\epsilon), \tag{23}$$

where N is a normalisation factor; ϵ is responsible for a linear, residual, long-range background; and \mathcal{K} is the Coulomb correction [24]:

$$\mathcal{K}(q; \alpha, R) = \frac{\int D(\vec{r}) \left| \psi_q^{\text{Coul}}(\vec{r}) \right|^2 d^3\vec{r}}{\int D(\vec{r}) \left| \psi_q(\vec{r}) \right|^2 d^3\vec{r}}, \tag{24}$$

where $D(\vec{r})$ is the simplified spatial pair distribution, and $\psi_q^{\text{Coul}}(\vec{r})$ is the solution to the two-particle Schrödinger equation in the presence of a Coulomb potential. In this study, $\mathcal{K}(q; \alpha, R)$ for kaons is calculated by numerically employing the procedure used in Refs. [12,24,43]. The inclusion of other final-state contributions, such as the strong interaction, can resolve the possible underestimation regarding R and λ and overestimation regarding α of the Lévy parameters [44]. However, the statistical significance of such precise corrections turns out to be negligible in the context of the current measurement.

5. Results

As illustrated in Figure 2, the Coulomb-corrected Lévy distribution function is in agreement with the measured $C(q)$ over the entire q_{LCMS} range. The femtoscopic peak [18,19] and the Coulomb hole [42] are both observed as expected. The values of the normalisation factor (N) and the linear background factor (ϵ) are observed to be close to 1 and 0, respectively.

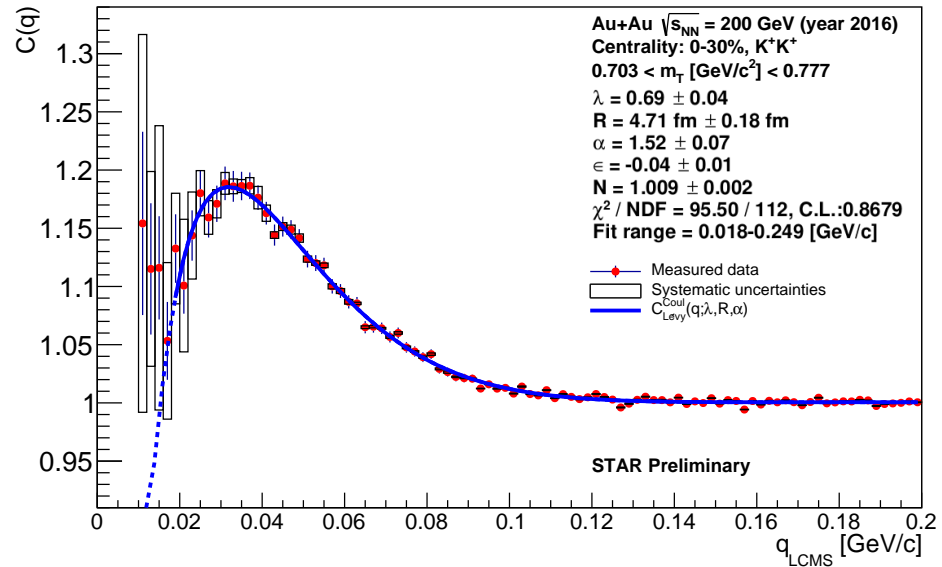


Figure 2. $C(q)$ as a function of q_{LCMS} for positively charged kaon pairs in the m_T range (703–777 MeV/ c^2) and the centrality range (0–30%). The red dots denote the measured data, and the blue lines (solid and dotted) denote the fit. The systematic uncertainties are shown as hollow rectangles.

The systematic uncertainties are obtained by combining the uncertainties arising from variations in the event- and pair-selection criteria, denoted by Δ_{cuts} , as mentioned above, and those arising out of variations to the range of the fit are denoted by Δ_{fits} . At this preliminary stage, systematic uncertainties arising out of variations in the track-selection criteria are not included. Thus, the final systematic uncertainties (Δ_{total}) are obtained as:

$$\Delta_{\text{total}} = \sqrt{(\Delta_{\text{fits}})^2 + (\Delta_{\text{cuts}})^2}. \quad (25)$$

Figure 3 shows the kaon homogeneity length (R), otherwise known as the Lévy scale, as a function of m_T . It is observed to exhibit large, systematic uncertainties, a very weak dependence on m_T and a possible decrease with respect to it, as reported in previous studies [2,3,6,8,14,45]. However, hydrodynamical studies predicting a decrease in the Lévy scale as a function of m_T are based on the Gaussian source assumption [2,3]. Hence, more investigations on this topic are in order. The extracted values of the Lévy scale in this charged-kaon analysis are also found to be similar to PHENIX’s like-sign pion results [9], with $R_{\pi} \sim 5\text{--}7$ fm for the m_T range of 600–700 MeV/ c^2 . A more detailed comparison of the m_T dependence of Lévy scales of different particle species could shed light on the origin of the appearance of Lévy-stable sources, given that, according to calculations based on hydrodynamics, species-independent m_T scaling was predicted in Ref. [46].

The intercept of the correlation function—the correlation strength, i.e., λ —is shown in Figure 4. Values extracted from the fits show that it is close to unity, as is to be expected based on the small fraction of decay kaons present in the system.

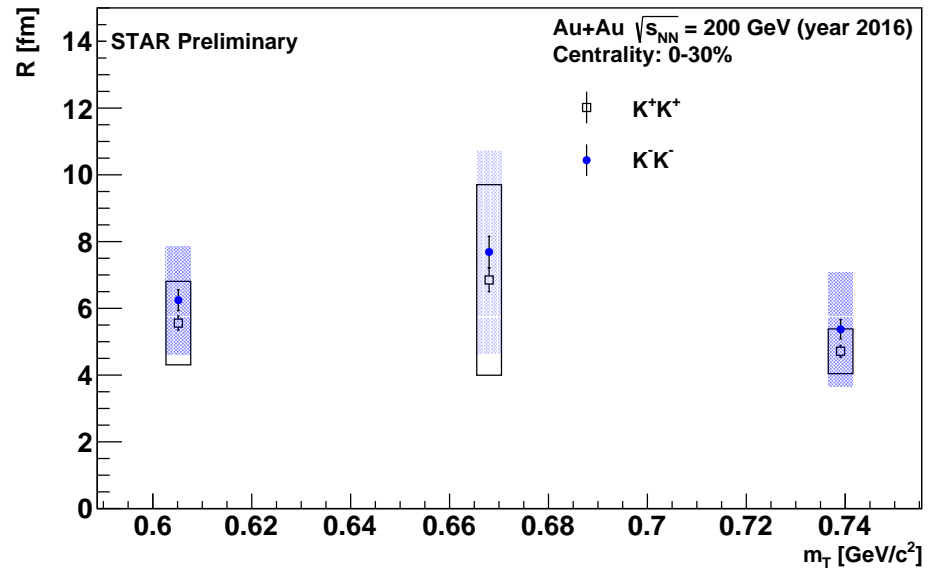


Figure 3. R as a function of m_T for 0–30% centrality. The hollow, blue squares denote positively charged kaon pairs and the solid, and blue circles denote negatively charged kaon pairs, along with their error bars. The systematic uncertainties are shown as hollow (K^+K^+) and shaded (K^-K^-) rectangles.

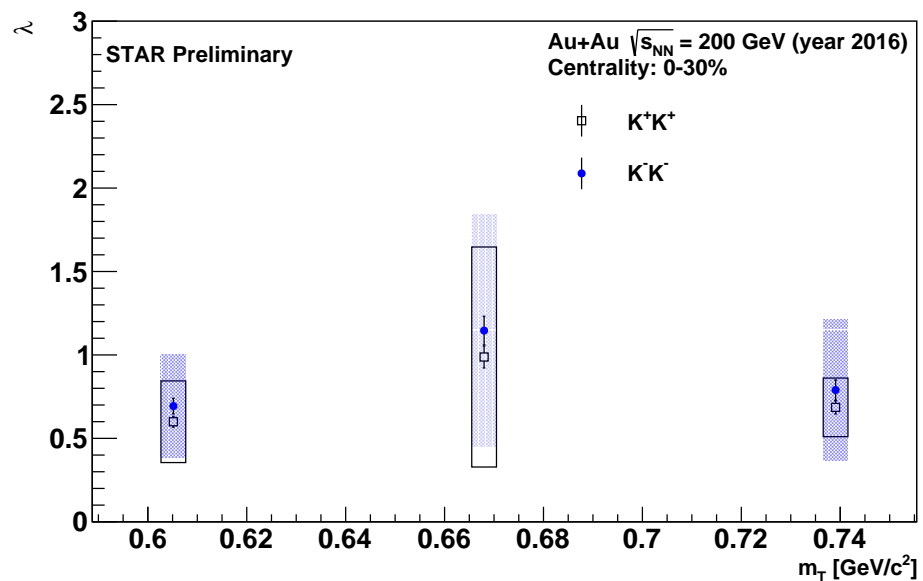


Figure 4. λ as a function of m_T for 0–30% centrality. The hollow, blue squares denote positively charged kaon pairs, and the solid, blue circles denote negatively charged kaon pairs, along with their error bars. The systematic uncertainties are shown as hollow (K^+K^+) and shaded (K^-K^-) rectangles.

The extent of the anomalous diffusion might be gleaned from the Lévy exponent (α) as shown in Figure 5, also illustrating the values corresponding to the Gaussian and Cauchy distributions, with dashed and dotted blue lines, respectively. The Lévy exponent is observed to have values between those two extremes, indicating power-law behaviour and the likely existence of anomalous diffusion. The extracted values of $\alpha \sim 1.0$ – 1.5 for kaons are similar to PHENIX’s pion results, with $\alpha_\pi \sim 1.2$ in the same transverse mass range. α_κ not being smaller than α_π hints at the existence of other factors on top of anomalous diffusion, contributing to the appearance of non-Gaussian source shapes. However, the current statistics prevent the drawing of more definitive conclusions.

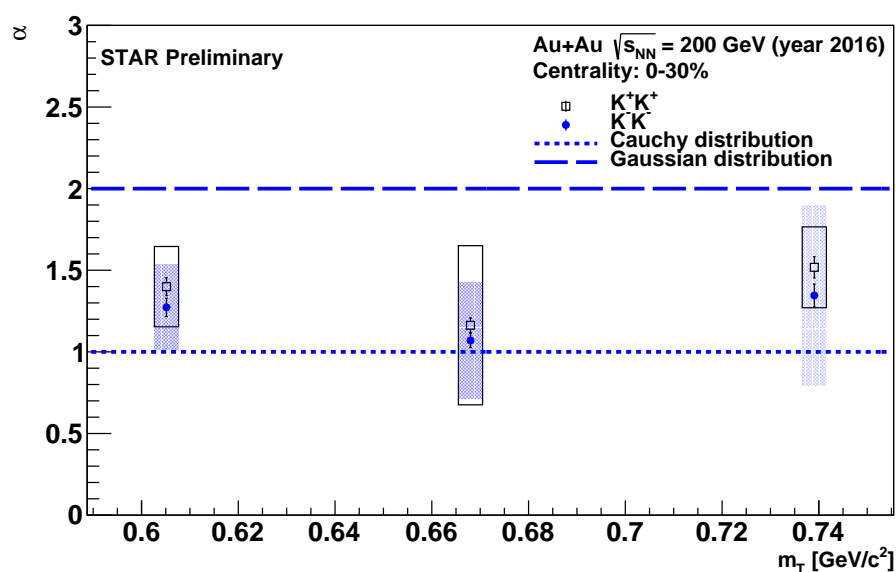


Figure 5. α as a function of m_T for 0–30% centrality. The hollow, blue squares denote positively charged kaon pairs, and the solid, blue circles denote negatively charged kaon pairs, along with their error bars. The systematic uncertainties are shown as hollow (K^+K^+) and shaded (K^-K^-) rectangles.

6. Summary

Preliminary analysis of data collected by STAR from RHIC’s 2016 BES $\sqrt{s_{NN}} = 200$ GeV Au + Au collisions suggests a non-Gaussian, Lévy-stable source shape for pairs of the identically charged kaons produced in the collisions. The Lévy-stability exponent α_κ is observed to be comparable to that of like-sign pion pairs obtained from PHENIX.

However, anomalous diffusion may not be solely responsible for the heavy tails observed in the source distributions, as suggested by the comparability of α_κ to α_π . It is to be noted that, a complete systematic uncertainty analysis, which is currently ongoing, is required to draw definitive conclusions about any and all claims made herein. Because Lévy-stable sources can arise in strongly interacting systems due to their proximity to the QCD critical end point at higher chemical potentials, similar studies at lower beam energies would likely strengthen the search for the QCD critical end point.

Funding: This project was funded, in part, by the TKP2021-NKTA-64 and K-136138 grants from the NKFIH, Hungary, and, in part, by the Department of Energy of the United States of America.

Data Availability Statement: Data publicly unavailable since publication is a communication.

Acknowledgments: This manuscript was prepared for a Special Issue corresponding to the Zimányi School Winter Workshop 2022. The author would like to thank the STAR collaboration and the people behind the RHIC framework, whose incessant efforts have produced every bit of data analysed as a part of this project. The author is also deeply indebted to Koushik Mandal for his invaluable help with discussions about the ROOT framework and the C++ programming language in particular and about the myriad intricacies of navigating the field of experimental heavy-ion physics in general.

Conflicts of Interest: The author declares no conflict of interest.

References

1. Lisa, M.; Pratt, S.; Soltz, R.; Wiedemann, U. Femtoscopy in relativistic heavy ion collisions. *Ann. Rev. Nucl. Part. Sci.* **2005**, *55*, 357–402. [[CrossRef](#)]
2. Makhlin, A.; Sinyukov, Y. Hydrodynamics of hadron matter under pion interferometric microscope. *Z. Phys. C* **1988**, *39*, 69. [[CrossRef](#)]
3. Csörgő, T.; Lörstad, B. Bose-Einstein correlations for three-dimensionally expanding, cylindrically symmetric, finite systems. *Phys. Rev. C* **1996**, *54*, 1390–1403. [[CrossRef](#)] [[PubMed](#)]
4. Csörgő, T.; Hegyi, S.; Novák, T.; Zajc, W. Bose-Einstein or HBT correlation signature of a second order QCD phase transition. *AIP Conf. Proc.* **2006**, *828*, 525–532. [[CrossRef](#)]

5. Oliinychenko, D. Overview of light nuclei production in relativistic heavy-ion collisions. *Nucl. Phys. A* **2021**, *1005*, 121754. [[CrossRef](#)]
6. Csanád, M.; Vargyas, M. Observables from a solution of 1 + 3 dimensional relativistic hydrodynamics. *Eur. Phys. J. A* **2010**, *44*, 473–478. [[CrossRef](#)]
7. Adams, J. et al. Pion interferometry in Au + Au collisions at $\sqrt{s_{NN}} = 200$ GeV. *Phys. Rev. C* **2005**, *71*, 044906. [[CrossRef](#)]
8. Adler, S. et al. Bose-Einstein correlations of charged pion pairs in Au + Au collisions at $\sqrt{s_{NN}} = 200$ GeV. *Phys. Rev. Lett.* **2004**, *93*, 152302. [[CrossRef](#)]
9. Adare, A. et al. Lévy-stable two-pion Bose-Einstein correlations in $\sqrt{s_{NN}} = 200$ GeV Au + Au collisions. *Phys. Rev. C* **2018**, *97*, 064911. [[CrossRef](#)]
10. Adler, S. et al. Evidence for a long-range component in the pion emission source in Au + Au collisions at $\sqrt{s_{NN}} = 200$ GeV. *Phys. Rev. Lett.* **2007**, *98*, 132301. [[CrossRef](#)]
11. Afanasiev, S. et al. Source breakup dynamics in Au + Au Collisions at $\sqrt{s_{NN}} = 200$ GeV via three-dimensional two-pion source imaging. *Phys. Rev. Lett.* **2008**, *100*, 232301. [[CrossRef](#)] [[PubMed](#)]
12. Sirunyan, A. et al. Bose-Einstein correlations in pp , pPb , and $PbPb$ collisions at $\sqrt{s_{NN}} = 0.9$ –7 TeV. *Phys. Rev. C* **2018**, *97*, 064912. [[CrossRef](#)]
13. Achard, P. et al. Test of the τ -model of Bose-Einstein correlations and reconstruction of the source function in hadronic Z-boson decay at LEP. *Eur. Phys. J. C* **2011**, *71*, 1648. [[CrossRef](#)]
14. Kincses, D.; Stefaniak, M.; Csanád, M. Event-by-event investigation of the two-particle source function in heavy-ion collisions with EPOS. *Entropy* **2022**, *24*, 308. [[CrossRef](#)] [[PubMed](#)]
15. Lednický, R. Correlation femtoscopy: Origins and achievements. *Phys. Part. Nucl.* **2020**, *51*, 221–226. [[CrossRef](#)]
16. Bose, S. Plancks gesetz und lichtquantenhypothese. *Z. Phys.* **1924**, *26*, 178–181. [[CrossRef](#)]
17. Einstein, A. Quantentheorie des einatomigen idealen gases. *Sitzungsber. Preuss. Akad. Wiss. Phys. Math. Kl.* **1925**, *1*, 3–14.
18. Goldhaber, G.; Fowler, W.; Goldhaber, S.; Hoang, T.; Kalogeropoulos, T.; Powell, W. Pion-pion correlations in antiproton annihilation events. *Phys. Rev. Lett.* **1959**, *3*, 181–183. [[CrossRef](#)]
19. Goldhaber, G.; Goldhaber, S.; Lee, W.; Pais, A. Influence of Bose-Einstein statistics on the antiproton-proton annihilation process. *Phys. Rev.* **1960**, *120*, 300–312. [[CrossRef](#)]
20. Hanbury-Brown, R.; Twiss, R. A new type of interferometer for use in radio astronomy. *Lond. Edinb. Dublin Philos. Mag. J. Sci.* **1954**, *45*, 663–682. [[CrossRef](#)]
21. Hanbury-Brown, R.; Twiss, R. Correlation between photons in two coherent beams of light. *Nature* **1956**, *177*, 27–29. [[CrossRef](#)]
22. Hanbury-Brown, R.; Twiss, R. A test of a new type of stellar interferometer on Sirius. *Nature* **1956**, *178*, 1046–1048. [[CrossRef](#)]
23. Yano, F.; Koonin, S. Determining pion source parameters in relativistic heavy-ion collisions. *Phys. Lett. B* **1978**, *78*, 556–559. [[CrossRef](#)]
24. Csanád, M.; Lökös, S.; Nagy, M. Expanded empirical formula for Coulomb final state interaction in the presence of Lévy sources. *Phys. Part. Nucl.* **2020**, *51*, 238–242. [[CrossRef](#)]
25. Csörgő, T.; Lörstad, B.; Zimányi, J. Bose-Einstein correlations for systems with large halo. *Z. Phys. C* **1996**, *71*, 491–497. [[CrossRef](#)]
26. Nolan, J. Parameterizations and modes of stable distributions. *Stat. Probab. Lett.* **1998**, *38*, 187–195. [[CrossRef](#)]
27. Csörgő, T.; Hegyi, S.; Novák, T.; Zajc, W. Bose-Einstein or HBT correlations and the anomalous dimension of QCD. *Acta Phys. Polon. B* **2005**, *36*, 329–337.
28. Csanád, M.; Csörgő, T.; Nagy, M. Anomalous diffusion of pions at RHIC. *Braz. J. Phys.* **2007**, *37*, 1002–1013. [[CrossRef](#)]
29. Csörgő, T. Correlation probes of a QCD critical point. *PoS* **2008**, *HIGH-PTLHC08*, 027. [[CrossRef](#)]
30. El-Showk, S.; Paulos, M.; Poland, D.; Rychkov, S.; Simmons-Duffin, D.; Vichi, A. Solving the 3d Ising model with the conformal bootstrap II. c-minimization and precise critical exponents. *J. Stat. Phys.* **2014**, *157*, 869–914. [[CrossRef](#)]
31. Rieger, H. Critical behaviour of the three-dimensional random-field Ising model: Two-exponent scaling and discontinuous transition. *Phys. Rev. B Condens. Matter* **1995**, *52*, 6659–6667. [[CrossRef](#)] [[PubMed](#)]
32. Halasz, M.; Jackson, A.; Shrock, R.; Stephanov, M.; Verbaarschot, J. Phase diagram of QCD. *Phys. Rev. D* **1998**, *58*, 096007. [[CrossRef](#)]
33. Stephanov, M.; Rajagopal, K.; Shuryak, E. Signatures of the tricritical point in QCD. *Phys. Rev. Lett.* **1998**, *81*, 4816–4819. [[CrossRef](#)]
34. Lacey, R. Indications for a critical point in the phase diagram for hot and dense nuclear matter. *Nucl. Phys. A* **2016**, *956*, 348–351. [[CrossRef](#)]
35. Lacey, R.; Liu, P.; Magdy, N.; Schweid, B.; Ajitanand, N. Finite-size scaling of non-Gaussian fluctuations near the QCD critical point. *arXiv* **2016**, arXiv:1606.08071.
36. Metzler, R.; Klafter, J. The random walk's guide to anomalous diffusion: A fractional dynamics approach. *Phys. Rep.* **2000**, *339*, 1–77. [[CrossRef](#)]
37. Csörgő, T.; Hegyi, S.; Zajc, W. Bose-Einstein correlations for Lévy stable source distributions. *Eur. Phys. J. C* **2004**, *36*, 67–78. [[CrossRef](#)]
38. Kurgyis, B.; Kincses, D.; Nagy, M.; Csanád, M. Coulomb interaction for Lévy sources. *arXiv* **2023**, arXiv:2007.10173.
39. Adamczyk, L. et al. Beam-energy-dependent two-pion interferometry and the freeze-out eccentricity of pions measured in heavy ion collisions at the STAR detector. *Phys. Rev. C* **2015**, *92*, 014904. [[CrossRef](#)]
40. Kincses, D. Shape analysis of HBT correlations at STAR. *Phys. Part. Nucl.* **2020**, *51*, 267–269. [[CrossRef](#)]

41. Bowler, M. Coulomb corrections to Bose-Einstein corrections have greatly exaggerated. *Phys. Lett. B* **1991**, *270*, 69–74. [[CrossRef](#)]
42. Sinyukov, Y.; Lednicky, R.; Akkelin, S.; Pluta, J.; Erasmus, B. Coulomb corrections for interferometry analysis of expanding hadron systems. *Phys. Lett. B* **1998**, *432*, 248–257. [[CrossRef](#)]
43. Csanád, M.; Lökös, S.; Nagy, M. Coulomb final state interaction in heavy ion collisions for Lévy sources. *Universe* **2019**, *5*, 133. [[CrossRef](#)]
44. Kincses, D.; Nagy, M.; Csanád, M. Coulomb and strong interactions in the final state of Hanbury-Brown–Twiss correlations for Lévy-type source functions. *Phys. Rev. C* **2020**, *102*, 064912. [[CrossRef](#)]
45. Afanasiev, S. et al. Kaon interferometric probes of space-time evolution in Au + Au collisions at $\sqrt{s_{NN}} = 200$ GeV. *Phys. Rev. Lett.* **2009**, *103*, 142301. [[CrossRef](#)]
46. Csanád, M.; Csörgő, T. Kaon HBT radii from perfect fluid dynamics using the Buda-Lund model. *Acta Phys. Polon. Supp.* **2008**, *1*, 521–524.

Disclaimer/Publisher’s Note: The statements, opinions and data contained in all publications are solely those of the individual author(s) and contributor(s) and not of MDPI and/or the editor(s). MDPI and/or the editor(s) disclaim responsibility for any injury to people or property resulting from any ideas, methods, instructions or products referred to in the content.